Multiconfigurational Effects in Theoretical Resonance Raman Spectra

Yingjin Ma, Stefan Knecht,* and Markus Reiher*[a]

We analyze resonance Raman spectra of the nucleobase uracil in the short-time approximation calculated with multiconfigurational methods. We discuss the importance of static electron correlation by means of density-matrix renormalization group self-consistent field (DMRG-SCF) calculations. Our DMRG-SCF results reveal that a minimal active orbital space that leads to a qualitatively correct description of the resonance Raman spectrum of uracil should encompass parts of the σ/σ* bonding/anti-bonding orbitals of the pyrimidine ring. We trace these findings back to the considerable entanglement between the σ/σ* bonding/anti-bonding as well as valence π/π* orbitals in the excited-state electronic structure of uracil, which indicates non-negligible non-dynamical correlation effects that are less pronounced in the electronic ground state.

1. Introduction

Resonance Raman (RR) spectroscopy[1] is a selective spectroscopic technique because the resonance conditions act like a filter such that only certain peaks are selectively enhanced in the vibrational spectrum. This experimental advantage can even be exploited for selective theoretical approaches such as intensity tracking.[2] In RR spectroscopy the energy of the incident light of a given wavelength matches the energy of an electronic transition in a molecule. As a result, only those vibrational frequencies associated with the targeted electronic transition are visible in the RR spectrum. For a given molecule or part of a molecular complex, RR spectroscopy therefore provides selective access to information about the excited-state structure and dynamics, see the combined experimental and theoretical study in Ref. [3] for an example. Theoretical calculations of RR spectra are often useful for the determination of these properties, including, for example, transition moments.[4,5] A comparison of calculated and measured RR spectra can be helpful to benchmark theoretical models and computational approaches to calculate RR spectra.[3,5–20]

Starting out from the Kramers, Heisenberg, and Dirac expression for the Raman polarizability tensor,[21,22] the calculation of RR intensities proceeds usually in either a time-independent or time-dependent framework, see, for example, Refs. [1, 10, 11, 14, 18, 20] (and literature references in these papers) and Refs. [7, 23, 24]. In this work, we follow the time-independent approach where we exploit the Kramers–Kronig (KK) transform relationship, which provides a connection between the polarizability and optical absorption spectrum.[7,8,10] Working within the Born–Oppenheimer approximation, we consider for the calculation of RR intensities 1) only Cotton scattering, that is, Herzberg–Teller vibronic couplings are neglected, and further assume that 2) only one electronically excited state is in resonance, 3) the vicinity of local minima on the ground- and excited-state potential energy surfaces is harmonic, 4) ground- and excited-state normal modes are identical as are their frequencies, commonly referred to as independent mode displaced harmonic oscillator (IMDHO) model, 5) the normal coordinates of the ground and excited states differ only in their equilibrium positions such that Duschinsky rotations do not play a role. These assumptions greatly simplify the calculation of RR intensities within the transform theory approach[7] as was discussed in detail in a landmark paper by Neugebauer and Hess.[10] Moreover, we do not take into account solvation effects, which do not appear to play a major role for a qualitatively correct description of the characteristic peaks in the RR spectrum of uracil.[17]

In previous studies on the RR spectrum of uracil in the gas phase,[7,8,10,17] the best agreement between the experimentally measured spectrum targeting the first bright spin-singlet excitation and theoretical ab initio predictions was obtained for Hartree–Fock/configuration interaction singles (HF/CIS). By contrast, density functional theory (DFT)/time-dependent DFT (TDDFT) calculations yielded a large overestimation of the peak intensity of the highest lying C=O stretching vibrational mode. However, in contradiction to most other (gas-phase) calculations,[17,25–29] which determine the first bright transition to occur from the electronic ground state (S_0) to the second excit-

[a] Dr. Y. Ma, Dr. S. Knecht, Prof. Dr. M. Reiher
ETH Zürich
Laboratorium für Physikalische Chemie
Vladimir-Prelog-Weg 2, 8093 Zürich (Switzerland)
E-mail: stefan.knecht@phys.chem.ethz.ch
        markus.reiher@phys.chem.ethz.ch

ed spin-singlet state S₂, HF/CIS predicted the bright transition to be of $S_0 \rightarrow S_1$ character.[7,10] In view of the latter, the rather unexpected accuracy of HF/CIS may be a result of a fortuitous cancellation of errors originating in particular from an unbalanced treatment of non-dynamical and dynamical electron correlation effects[10] rather than from basis set incompleteness (see, for example, Ref. [30] for a basis set study on HF/CIS excitation energies of uracil).

To understand the dynamical and non-dynamical electron correlation on the RR spectrum of uracil in the gas phase, we calculate RR spectra in the short-time approximation based on excited-state gradients from complete active space (CAS) self-consistent field (CASSCF),[31–33] CAS perturbation theory to second order (CASPT2),[34,35] and density-matrix renormalization group self-consistent field (DMRG-SCF)[36,37] wave functions. In the latter case, we further rationalize the different choices of active orbital spaces in terms of orbital entanglement measures, which allows us to systematically improve the calculated RR spectrum.

In contrast to a traditional CASSCF *ansatz*, which suffers from an exponential growth[38] of the underlying full configuration interaction expansion with respect to an increasing number of electrons N distributed over L active orbitals, CAS(N,L), the DMRG approach[39–42] in quantum chemistry[43–55] allows one to approximate CAS-type wave functions up to chemical accuracy with polynomial scaling. Combined with a self-consistent-field orbital optimization *ansatz*, DMRG-SCF,[36,37] active orbital spaces as large as five to six times the limit of traditional CASSCF(18,18) are feasible. Although the selection of suitable (large) active orbital spaces requires careful consideration, it may be automated.[56,57]

This paper is organized as follows. In Section 2, we provide a brief introduction to the key elements that are needed to calculate a RR spectrum for a DMRG-SCF wave function within the (time-independent) transform theory approach. Computational details are given in Section 3. In Section 4, we discuss the absorption and RR spectra of uracil obtained for our selection of ab initio approaches. Based on a sequence of DMRG-SCF data for increasingly larger active orbital spaces, we elucidate the connection between orbital entanglement and relative peak intensities in the RR spectrum of uracil.

2. Computational Methodology

Given the assumptions stated in the Introduction, the relative intensity for the fundamental transition $i_j^{1 \leftarrow 0}(\omega_s)$ of the j-th normal mode is given by Equation (1):[7,10]

$$i_j^{1 \leftarrow 0}(\omega_s) = \omega_L \omega_s^3 |\mathbf{\mu}_{0s}^{el}|^4 \left(\frac{\Delta_j^2}{2}\right) |\Phi(\omega_L) - \Phi(\omega_L - \Omega_j)|^2 \quad (1)$$

where ω_L is the laser excitation frequency, $\omega_s = \omega_L - \Omega_j$ is the frequency of the scattered light, Ω_j is the harmonic vibrational frequency, and Δ_j is the normal-mode displacement in the excited-state equilibrium structure. In the present study, we only consider contributions to the RR spectrum from the second

spin-singlet excited state [S₂, that is, $s=2$ in Eq. (1)] of uracil, which has, by orders of magnitude, the largest electronic transition dipole moment $\mathbf{\mu}_{02}^{el}$ in the lower-lying excited-state spectrum of uracil.[58] Within the IMDHO model, we obtained the normal mode shifts Δ_j by taking the partial derivative of the excited-state electronic energy E_{el}^{ex} with respect to a dimensionless ground-state normal coordinate q_j at the ground-state equilibrium position, $q_j = 0$ [Eq. (2)]:

$$\left(\frac{\partial E_{el}^{ex}}{\partial q_j}\right)_{q_j=0} = \Omega_j(q_j - \Delta_j)|_{q_j=0} = -\Omega_j \Delta_j \quad (2)$$

Then, explicit knowledge of the corresponding minimum excited-state geometry is not needed. Details of the explicit form of the functions $\Phi(\omega_L)$ $(\Phi(\omega_L - \Omega_j))$,[7] which enter the calculation of the relative intensity $i_j^{1 \leftarrow 0}(\omega_s)$ in Equation (1), can be found in Ref. [10]. Their evaluation in the DNR program[59] by Neugebauer follows the approach outlined in Ref. [10].

Moreover, for a general discussion on the calculation of state-specific gradients from DMRG-SCF wave functions, we refer the reader to the recent work of Hu and Chan.[60]

3. Computational Details

We calculate the excited-state energy derivatives with respect to the ground-state normal modes [cf. Eq. (2)] for the S₂ state from analytic Cartesian gradients that are subsequently transformed into the basis of normal coordinates.

The chemical structure and atomic indices of uracil are given in Figure 1, which agree with the atomic numbering of Ref. [17]. All calculations were carried out with the aug-cc-pVTZ basis set.[61,62] Following the work of Sun and Brown,[17] we optimized the ground-state equilibrium structure of uracil with PBE0[63–65] in Gaussian 09[66] and subsequently calculated the vibrational frequencies for the optimized structure. A detailed study of the density-functional and basis-set dependence

Figure 1. The chemical structure of uracil with atomic numbering.

of the vibrational spectrum (frequencies as well as intensities) for uracil was conducted in Ref. [67], which showed that PBE0/aug-cc-pVTZ can give an overall good accuracy in comparison to experimental data. For the calculation of the HF/CIS and PBE0 excited-state gradients, Turbomole 6.5[68] was employed whereas analytical CASSCF and DMRG-SCF as well as numerical CASPT2 excited-state gradients were calculated with a development version of Molcas,[38] which provides an interface to our DMRG program QCMaquis.[54,69–71] For this purpose, we implemented analytical state-specific gradients into the QCMaquis framework. State-averaged calculations for the three lowest spin-singlet states allowed us to identify the bright excited state and obtain pre-optimized orbitals, from which the state-specific calculations are started to calculate the gradient for
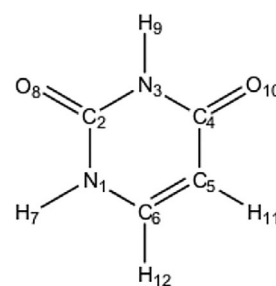
the bright excited state. In all DMRG-SCF calculations, the number of renormalized block states m, which determines amongst other factors the orbital ordering the accuracy of a DMRG calculation,[72] was set to $m = 1000$. Furthermore, all calculations were carried out with an optimized orbital ordering based on the Fiedler vector.[52–54,73]

For the CASSCF/CASPT2 results, we performed multistate CASPT2 calculations to obtain excitation energies and state-specific calculations for the excited-state gradients. With the Cartesian gradients at hand, we calculated the transformed gradients in the basis of normal coordinates with Transgrad,[74] from which the DNR program[59] calculates the RR spectra. The energy of the incident photon was chosen to be 266 nm, which is the wavelength of the frequency-doubled Nd-YAG laser used in experiments.[7,75] The full width at half maximum (fwhm) is set to 30 cm^{-1}, which is selected to be equal to that of the single peak in the experimental resonance Raman spectra.[17,75] Assuming a Gaussian broadening, the excitation wavelength to model the first absorption band of the experimental spectrum was set for all calculations to 5.29 eV, corresponding to the excitation energy obtained from TDDFT calculations with the PBE0 functional and an aug-cc-pVTZ basis set. No symmetry restrictions were imposed, that is, all calculations were carried out without any symmetry restrictions, that is, in C_1 point group symmetry.

4. Results and Discussions

4.1. Equilibrium Structure and Normal Modes

As we employ the same computational setup (PBE0/aug-cc-pVTZ) as Sun and Brown[17] to optimize the ground-state equilibrium structure of uracil, we confirmed that our optimized structure, the vibrational frequencies, and the normal modes match to numerical accuracy, for example, to within 1 cm^{-1} for

the vibrational frequencies, with the data provided in Table 1 and the Supporting Information of Ref. [17]. Note that Table 1 in Ref. [17] apparently contains a misprint for the vibrational frequency ω of normal mode 24 and the scaling factor for frequencies higher than 1000 cm^{-1}, which should read $\omega = 1622$ cm^{-1} and 0.9568, respectively. The correct values were reported in Table 5 of that paper and subsequently entered their calculation of the RR spectra. Concerning the following analysis and discussion of the RR spectra in Section 4.4, we therefore refer the reader to Section 3.1 and Table 1 of Ref. [17] where a list of all normal modes and vibrational frequencies that are necessary to analyze the experimental RR spectrum of uracil is available.

4.2. Active Orbital Space Considerations

The selection of the active space is a crucial step for CASSCF and DMRG-SCF calculations, but may be automated.[56,57] In a previous study by Mercier et al.,[76] a CAS with 14 electrons distributed in ten orbitals, CAS(14,10), was chosen for the CASSCF calculations and a smaller CAS(12,9) (see below) was selected for their subsequent CASPT2 calculations whereas we kept, in this work, the CAS(14,10) as our reference space for the CASPT2 calculations. The CAS(14,10) included the occupied π and unoccupied π* orbitals as well as the lone-pair electrons of the two n_O orbitals. Moreover, as discussed in Ref. [76], excitations from the S_0 ground to the low-lying spin-singlet S_1 and S_2 excited states and subsequent excited-state structure relaxation entails considerable changes of the skeletal C4=O10, C4—C5, and C5—C6 bonds. Accordingly, all skeleton σ/σ* orbitals are included in the active orbital space for our reference DMRG-SCF calculation. The resulting complete set of active orbitals that comprise the CAS(30,26) are summarized in Figure 2. We note in passing that this CAS size is far beyond the realm of standard CASSCF approaches, and hence DMRG is
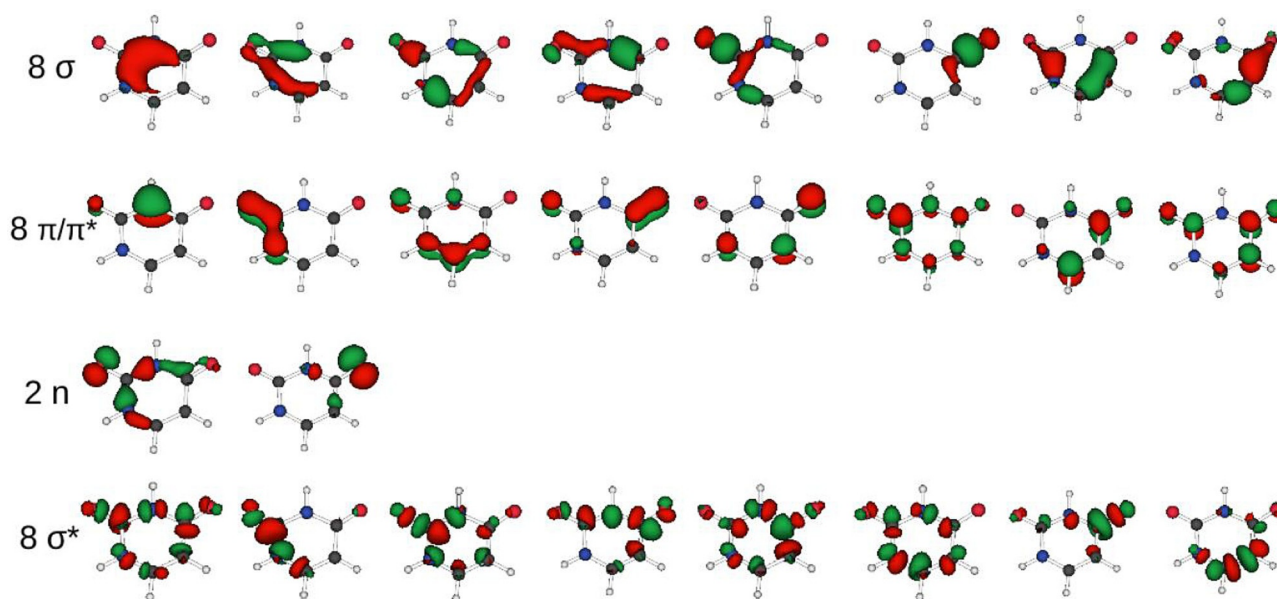

Figure 2. Valence active orbitals of uracil as obtained from a DMRG-SCF(30,26) calculation carried out with C_1 point group symmetry.

the method of choice. In addition, low-lying Rydberg orbitals may have to be included as it is known that Rydberg-like excited states can potentially interact with valence excited states in aromatic molecules.[77,78] To this end, we identified a set of 3p- and 4p-like Rydberg orbitals by manual inspection of their shapes and a population analysis of the initial wave function as they typically only overlap very little with the corresponding unoccupied valence (σ^*/π^*) orbitals.

4.3. Vertical Excited-State Spectrum of Uracil

4.3.1. Energies

Table 1 compiles the vertical $S_0 \rightarrow S_1$ and $S_0 \rightarrow S_2$ excitation energies and the excited-state energy gap $\Delta_{S_2-S_1}$ obtained here from different ab initio approaches. The vertical excitation energy of 5.29 eV for the $S_0 \rightarrow S_2$ transition from the PBE0 calculation is remarkably close to the experimental value (5.08 eV)[59]

Table 1. Vertical excitation energies for the lowest-lying spin-singlet states S_1 and S_2 of uracil and the excitation energy gap $\Delta_{S_2-S_1}$ calculated with various electronic structure methods (see text for details). All values are given in eV.

Method	S_1	S_2	$\Delta_{S_2-S_1}$
HF/CIS	6.40	6.43	0.03
PBE0	4.81	5.29	0.48
CASSCF(14,10)	5.02	6.60	1.58
CASSCF(14,10)/CASPT2	5.00	5.10	0.10
DMRG-SCF(14,18)	5.22	6.04	0.82
DMRG-SCF(14,26)	5.16	5.91	0.75
DMRG-SCF(30,26)	5.40	6.30	0.90
DMRG-SCF(18,23)	5.39	6.05	0.66
experiment	4.68[a]	5.08[b]	0.40

[a] Ref. [80], estimated from single-crystal absorption spectrum measurements for 1-methyl-uracil. [b] Ref. [58], measured in the gas phase.

and the energy gap $\Delta_{S_2-S_1}$ of 0.48 eV compares well with the experimental estimate of 0.40 eV. Note that these findings are in line with the earlier work of Improta and Barone.[79] By contrast, HF/CIS reduces $\Delta_{S_2-S_1}$ to 0.03 eV, which is considerably smaller than the gap of 0.42 eV reported by Neugebauer and Hess for HF/CIS with a 6-31G* basis set.[10] Moreover, HF/CIS/aug-cc-pVTZ overestimates the experimental vertical excitation energy for the $S_0 \rightarrow S_2$ transition by 1.35 eV. Similarly, CASSCF with a CAS(14,10) active orbital space overshoots the latter vertical transition by approximately 1.50 eV whereas the $\Delta_{S_2-S_1}$ gap increases to almost 1.6 eV. CASSCF/CASPT2 based on the same CAS(14,10) yields a large correction of 1.5 eV for the $S_0 \rightarrow S_2$ excitation energy, whereas the vertical $S_0 \rightarrow S_1$ transition energy hardly changes. The large correction observed for CASSCF/CASPT2 compared with CASSCF indicates 1) a lack of (differential) dynamical correlation effects and 2) the inadequacy to describe all non-dynamical correlation on an equal footing, which appears to be particularly important for an adequate description of the S_2 state. The latter means in practice,

as shown by Roos et al.,[77] that the active space for the CASSCF orbital optimization should comprise at least all valence π orbitals and, in addition, ideally all Rydberg-type orbitals from potentially interfering low-lying Rydberg states.

In our DMRG-SCF calculations, we therefore augmented the starting CAS(14,10) active orbital space with eight Rydberg-type (3p-like) orbitals and 16 Rydberg-type (3p- and 4p-like) orbitals, which we denote as DMRG-SCF(14,18) and DMRG-SCF(14,26) in Table 1, respectively. Enlarging the CAS not only significantly improves the absolute vertical excitation energy for the S_2 state while only slightly increasing the $S_0 \rightarrow S_1$ transition energy but also reduces for DMRG-SCF(14,26) the gap $\Delta_{S_2-S_1}$ to more than half of its CASSCF value. Interestingly, the optimized orbitals from these two DMRG-SCF calculations show a slight mixing of the π and σ orbitals, which could indicate that some of the skeleton σ/σ^* orbitals play a (minor) role in the electronic excitation process.

To corroborate this hypothesis, we carried out DMRG-SCF calculations with a CAS(30,26) active orbital space. The CAS comprises eight π/π^*, two n, and 16 σ/σ^* orbitals, that is, the full-valence orbital space of uracil. As can be seen from the third-to-last row in Table 1, the inclusion of σ/σ^* orbitals in the CAS(30,26) leads to a reduction of $\Delta_{S_2-S_1}$ from about 1.6 eV (CAS(14,10)) to 0.9 eV. The closing gap is a result of a considerable upward shift by 0.4 eV of the vertical excitation energy to the S_1 state (further away from its estimated experimental value at approximately 4.7 eV, which was originally measured for 1-methyl-uracil)[80] together with a down shift for the vertical excitation energy to the S_2 state. Augmenting the CAS(30,26) with eight Rydberg-type orbitals (see above) led to convergence issues within our three-state average DMRG-SCF model with a low-lying singlet state of $n \rightarrow$ Rydberg excitation character being lower in energy than the (expected) S_2 excited state of dominating $\pi \rightarrow \pi^*$ excitation character. For this reason, we did not pursue these calculations further.

4.3.2. Excited-State Analysis

Figure 3 shows the entanglement diagram for the S_2 state obtained from a DMRG-SCF(30,26) calculation, which summarizes the single-orbital entropy $s_i(1)$[81,82] for each spatial orbital i and the mutual information I_{ij}.[83] The diagram representation follows Ref. [56]: the area of the red circles assigned to each orbital is proportional to the single-orbital entropy $s_i(1)$ of the respective orbital i whereas the line connecting two orbitals i, j denotes their mutual information value I_{ij}. The direct connection between orbital entanglement and non-dynamical electron correlation[84] allows us to analyze the active space in terms of non-dynamical electron correlation contributions originating from different orbital types and/or interactions. Inspecting Figure 3, we first note that the π/π^* orbitals (#9–16 in Figure 3) have the largest $s_i(1)$ values, with maxima for orbitals #13 and #14, namely the highest occupied and lowest unoccupied molecular orbitals, HOMO and LUMO, of uracil. These findings agree therefore very well with the known $\pi \rightarrow \pi^*$ HOMO–LUMO excitation character[58] of the S_2 state. Turning next to the mutual information, we find two distinct regions in
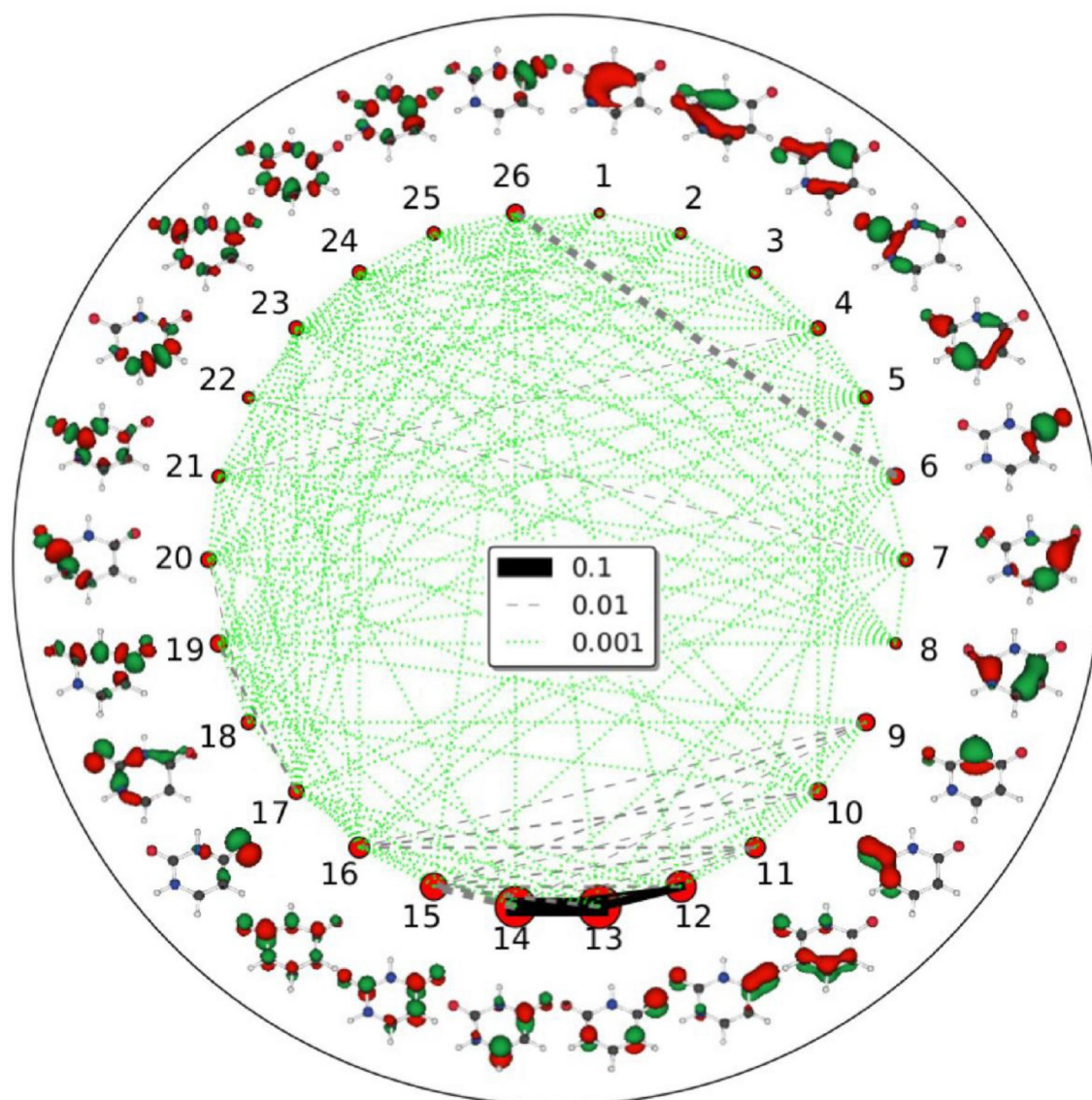
Figure 3. Entanglement diagram calculated from the DMRG-SCF(30,26) wave function of the S_2 excited state. All orbitals are aligned around the ring in the order #1–8 (σ), #9–16 (π/π^*), #17–18 (n), and #19–26 (σ^*). The area in the red circles indicates the magnitude of the single-orbital entropy $s_i(1)$. The line connecting two orbitals denotes their mutual information value I_{ij} where darker (from green to black) and thicker lines correspond to an increasing value of the mutual information.

the entanglement diagram with $I_{ij} > 0.01$: the first one (orbitals #1–18) comprises the σ, n, and π/π^* orbitals, whereas the second one (orbitals #19–26) consists of the σ^* orbitals. Both the noticeable mutual information between the π/π^* and n/σ^* orbitals as well as the mutual information between the σ/σ^* orbitals can be considered as a direct indication for the energetic stabilization of the S_2 state (see Section 4.3) upon enlarging the CAS with the skeleton σ/σ^* orbitals. Although there appears to be only weak mutual information, that is, $0.001 < I_{ij} < 0.01$ between the σ^* and π/π^* orbitals, the former is, however, important to appropriately describe a change of the σ-bonding structure of the pyrimidine skeleton after electronic excitation (see Section 4.2). In agreement with our entanglement analysis, the latter can be regarded as a predominant dynamical electron correlation effect.

Consequently, we defined a new active orbital space along the guidelines of Ref. [56], which we consider to be most appropriate from the point of view of taking into account nondynamic electron correlation in a balanced manner for the ground and low-lying excited states, while leaving the treatment of (differential) dynamical correlation effects to a post DMRG-SCF approach. The resulting CAS(18,23) comprises the eight π/π^* orbitals (which have the largest $s_i(1)$ values), the lone-pair of the carbonyl C4=O10 oxygen (from which the excitation occurs in the $n \rightarrow \pi^*$ S_1 state), six σ/σ^* orbitals corresponding to the skeleton C4=O10, C4–C5, C5–C6 bonding and anti-bonding orbitals (as indicated by I_{ij} values > 0.01) as well as eight additional Rydberg-type orbitals. Although still yielding too high vertical excitation energies (see Table 1), the excited-state gap $\Delta_{S_2-S_1}$ for DMRG-SCF(18,23) is the smallest one

(0.66 eV) of the CASSCF/DMRG-SCF series and closest to the PBE0 and estimated experimental values.

4.4. Resonance Raman Spectra

The gas-phase RR spectra calculated in this work are shown in Figure 4 and Figure 5 and compared with the experimental spectrum.[75] All spectra are calculated at the PBE0 ground-state equilibrium structure. The excited-state gradients for the S_2 state, which are required to calculate the relative RR intensities within the short-time approximation, were obtained with different methods as indicated in the individual panels of

Figure 4 and Figure 5. The numbering and characterization of the normal modes follows the assignment compiled in Table 1 of Ref. [17].

As we consider the same computational setup for our PBE0/aug-cc-pVTZ calculations as Sun and Brown,[17] we were able to reproduce their gas-phase RR spectrum (cf. Figure 2 in Ref. [17]). It compares reasonably well with the experimental RR spectrum shown in the uppermost panel of Figure 4, with the notable exception of the normal mode #26 (C2=O8 stretching mode) at 1752 cm^{-1}, the intensity of which is largely overestimated. As discussed in Ref. [17], employing long-range corrected density functionals leads to a significant reduction of
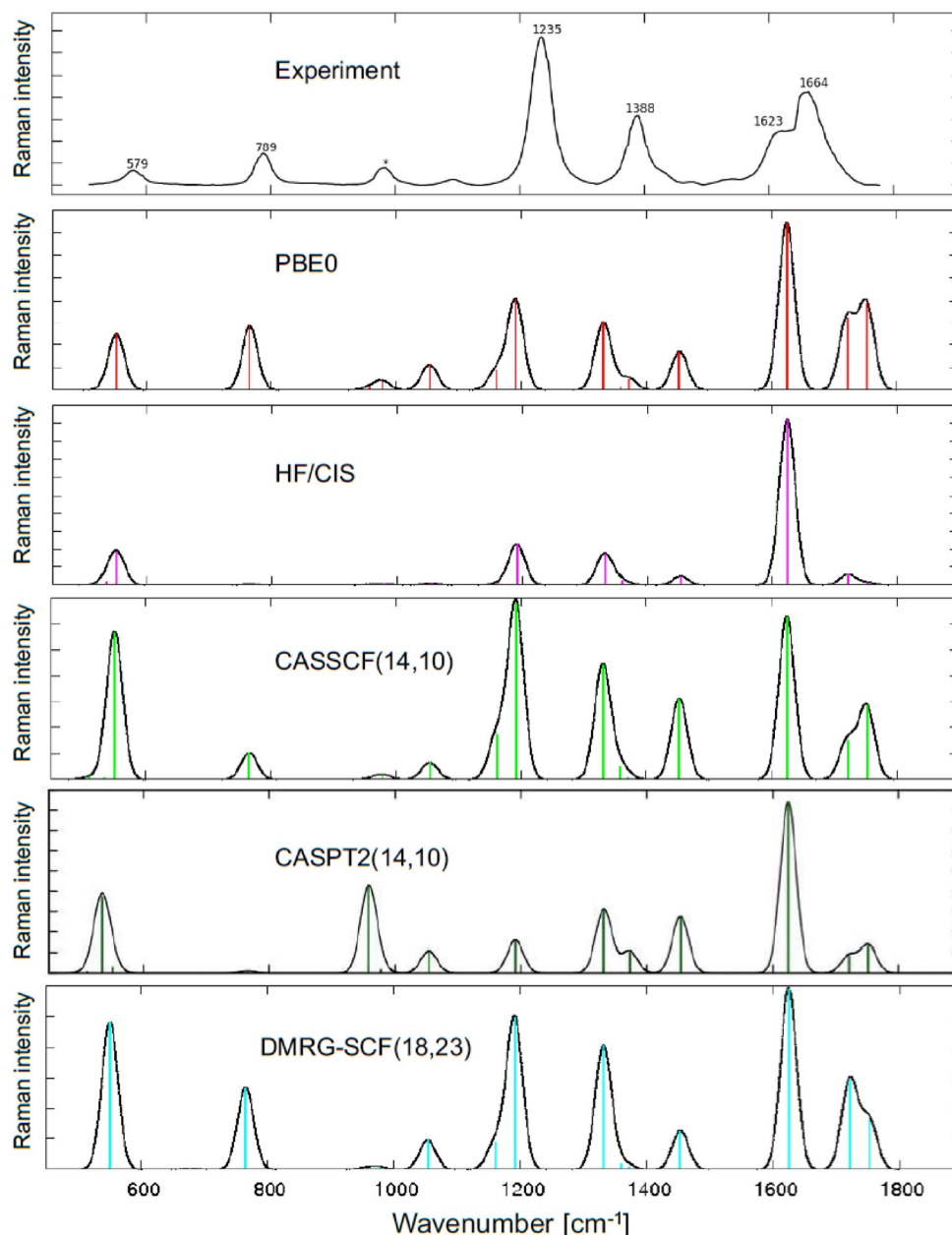

Figure 4. RR spectra of uracil in the gas phase. Intensities are given in arbitrary units. From top to bottom: Experiment spectrum reproduced from data taken from Ref. [75], HF/CIS, CASSCF/CASPT2(14,10), and DMRG-SCF(18,23). Frequencies for the ground state are taken from our PBE0/aug-cc-pVTZ calculation and scaled by 0.9776 (frequencies lower than 1000 cm^{-1}) and 0.9568 (frequencies higher than 1000 cm^{-1}), see Ref. [87]. We applied a Gaussian broadening with full-width half-maximum of 30 cm^{-1}. The 0.4 M sulfate internal standard peak in the experimental spectrum[75] is indicated by an asterisk.
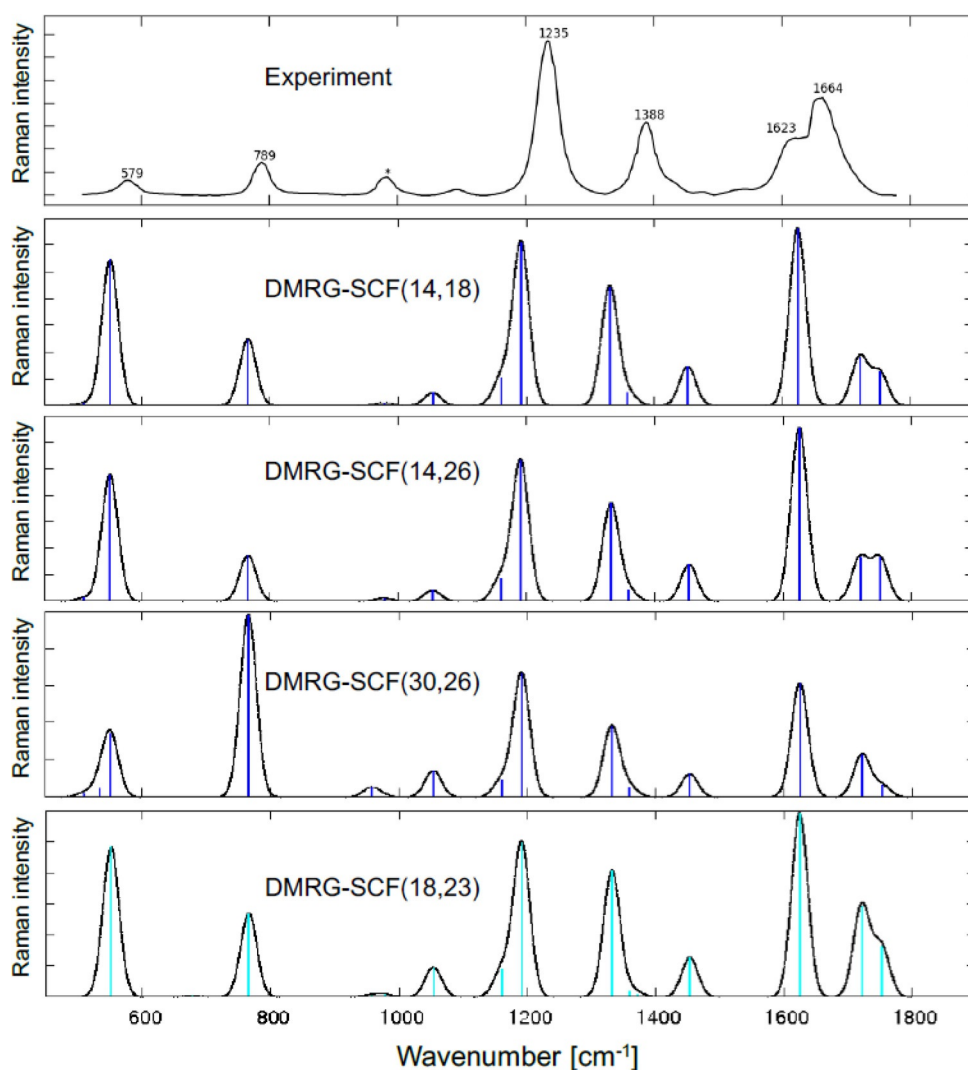
Figure 5. RR spectra of uracil in the gas phase. Intensities are given in arbitrary units. From top to bottom: Experiment spectrum reproduced from data taken from Ref. [75], DMRG-SCF(14,18), DMRG-SCF(14,26), DMRG-SCF(30,26), and DMRG-SCF(18,23). Frequencies for the ground state are taken from our PBE0/aug-cc-pVTZ calculation and scaled by 0.9776 (frequencies lower than 1000 cm^{-1}) and 0.9568 (frequencies higher than 1000 cm^{-1}), see Ref. [87]. We applied a Gaussian broadening with full-width half-maximum of 30 cm^{-1}. The 0.4 M sulfate internal standard peak in the experimental spectrum[75] is indicated by an asterisk.

the peak intensity, which could indicate that this mode corresponds to the unassigned peak centering around 1800 cm^{-1} in the experimental spectrum of Ref. [7].

Concerning the most intense vibrational bands lower than 1000 cm^{-1} corresponding to the ring bending modes #7 (551 cm^{-1}) and #12 (765 cm^{-1}), we find that, with the exception of PBE0, none of the methods compiled in Figure 4 yields a qualitatively correct relative intensity ratio in comparison to the experimental bands. All wave-function based approaches overestimate (underestimate) the intensity of the bending mode #7 (#12) among which DMRG-SCF(18,23) shows the best relative intensity ratio of both. By contrast, CASPT2 and in particular HF/CIS, which, in previous works,[7,8,10] yielded with a 6-31G* basis set a qualitatively correct intensity ratio, appear to wrongly predict a nearly zero intensity for the bending mode #12.

Following UV irradiation, uracil forms either a cyclobutyl photodimer or a photohydrate as photochemical products, with the latter being the major photoproduct in contrast to thymine where the former is produced in excess.[85] The formation of either photoproduct implies that the C5=C6 double bond of the parent uracil molecule is turned into a single bond along with sp^3-hybridized carbon atoms at C5 and C6.[75] Consistent with these findings, the most significant, intense bands in the experimental RR spectrum of uracil at frequencies higher than 1000 cm^{-1} have been identified as ring stretches coupled to primarily C5–H11 and C6–H12 bending modes at 1235 cm^{-1}, a ring stretching band at 1388 cm^{-1}, and a C5=C6 stretching mode at 1623 cm^{-1}.[75] Interestingly, the second most intense band in the experimental spectrum at 1664 cm^{-1} corresponds predominantly to a C4=O10 stretching mode,[75] which does not appear to be of any relevance for the photo-

chemical reaction coordinate, leading to the formation of either photoproduct.

Based on the PBE0 normal mode analysis compiled in Table 1 of Ref. [17], the bands #18 and #19 in the calculated spectra at 1159 cm^{-1} and 1187 cm^{-1} can be identified as ring stretching modes coupled to hydrogen bending modes (see above). The absolute intensity of their resulting broadened peak is not only largely underestimated for HF/CIS, CASPT2, and, to a lesser extent, for PBE0 but also its intensity ratio in comparison to the intensity distribution of the ring stretching and bending modes #20–23 between 1331 cm^{-1} and 1452 cm^{-1}. By contrast, DMRG-SCF, independent of the composition of the active orbital space (cf. Figure 5), as well as CASSCF predict a high-intensity peak for the bands #18 and #19 with a relative intensity ratio compared with the modes #20–23 that is in good agreement with the experimental reference spectrum. Note that, as pointed out by Sun and Brown,[17] the low-intensity peak of the combined ring stretching and bending mode #23 at 1452 cm^{-1}, which we also observe in all calculated spectra, could have been masked under the long tail of the experimental peak at 1388 cm^{-1} and hence escape assignment in the experimental spectrum. Moreover, with the exception of CASSCF, all our computational approaches yield as the most intense band of the RR spectrum of uracil the C5=C6 stretching mode at 1622 cm^{-1}, which appears to be in contradiction to the relative intensity ratio compared with the modes #18 and #19 as observed in the experiment. In addition, both C=O stretching modes (#25 and #26) are too weak in intensity compared with the C5=C6 stretching mode, although the relative ratio between both modes #25 and #26 is well captured by DMRG-SCF in contrast to all other electronic-structure models considered in this work. As indicated earlier, HF/CIS performs particularly poorly, which seems all the more surprising as it worked reasonably well in a number of earlier studies on uracil.[7,8,10] Recalling that the experimental spectrum is recorded in an aqueous solution of uracil, a possible origin for the generally observed discrepancies concerning the three modes #24–26 could be rooted in explicit hydrogen bonding between water and the carbonyl groups of uracil.[17] It was found earlier in a theoretical microsolvation study of uracil[86] that explicit hydrogen bonding leads to a distinct red-shift of the carbonyl mode frequencies whereas the C5=C6 stretching mode frequency is hardly affected.

Turning finally to a comparison of our selected CAS models for DMRG-SCF in Figure 5 with respect to their ability to (qualitatively) predict the RR spectrum of uracil, we note two distinct changes in the peak intensity distributions across all RR spectra: 1) the intensity ratio between the two main peaks below frequencies of 1000 cm^{-1}, namely modes #7 and #12, and 2) the intensity ratio between the ring stretching/bending modes #18 and #19 at approximately 1200 cm^{-1} and the C5=C6 stretching mode at 1622 cm^{-1}.

Considering first the lower frequency bands, we find that augmenting the starting CAS(14,10), which we considered in the CASSCF calculations above, by Rydberg-type orbitals decreases the intensity ratio between both ring bending/ring stretching modes. However, only by including the full set of

valence (σ, σ^*, π/π^*, and n_O) orbitals in the DMRG-SCF(30,26) calculation is there a clear inversion of the intensity ratio between both delocalized modes, which is in qualitative agreement with the experimental intensity ratio. By contrast, taking into account only part of the σ, σ^* skeleton orbitals in the DMRG-SCF(18,23) calculation reverts the intensity ratio, although we find a much better relative distribution compared with the starting CAS(14,10) reference data (cf. CASSCF spectrum in Figure 4). As discussed in Section 4.3.2, the entanglement analysis for the S$_2$ state clearly showed a mutual information value >0.001 between all σ/σ^* and π/π^* orbitals, respectively. Consequently, this could indicate non-negligible dynamic correlation effects comprising the whole valence orbital space, which are of particular importance for a qualitatively correct description of the intensity ratio between these lower, delocalized frequency modes.

Considering next the peak intensity ratio for the higher frequency modes, the addition of Rydberg-type orbitals appears to balance the intensity ratio towards the C5=C6 stretching mode (cf. the DMRG-SCF(14,18) and DMRG-SCF(14,26) spectra in Figure 5). This trend is, in agreement with the experimental peak intensity ratio, reverted for DMRG-SCF calculations with the full-valence CAS(30,26) space. Moreover, reducing the number of skeleton σ/σ^* orbitals in the DMRG-SCF(18,23) calculation appears to have a smaller effect on the peak intensity distribution of the higher frequency modes than was the case for the lower frequency modes.

In summary, we find that for all DMRG-SCF calculations considered here, the best qualitative agreement between the calculated and experimental RR spectrum can be obtained with the full-valence active orbital space CAS(30,26). Taking into further consideration the vertical excitation and excited-state entanglement analysis of Sections 4.3 and 4.3.2, respectively, we suggest that subsequent multireference calculations should start from a CAS(18,23) reference wave function. The latter not only provides a reasonable balance between capturing static and dynamic electron correlation but still reproduces correctly most of the experimental bands in the RR spectrum of uracil. The fact that dynamic electron correlation is of importance not only for obtaining a reasonable vertical excited-state spectrum (cf. Section 4.3) can be seen from a comparison of the CASSCF with the corresponding CASPT2 RR spectrum shown in Figure 4. We conclude by emphasizing that we did not take into account other effects, such as, for example, hydrogen bonding and/or Duschinsky rotations, for our analysis and interpretation of the calculated RR spectra of uracil in comparison to experiment. Except for the bands at frequencies around 1600–1700 cm^{-1}, recent works[17,75] showed that the latter effects play only a minor role concerning the peak positions and intensities of the most prominent bands in the RR spectrum of uracil.

5. Conclusions

In this work, we calculated within the short-time approximation the RR spectrum of uracil in the gas phase with TDDFT (PBE0 density functional) and different ab initio wave function

approaches including HF/CIS, CASSCF, CASPT2, and DMRG-SCF. For the latter, we explored various active orbital spaces, which were chosen according to electron correlation and quantum information measures of the valence orbital space of uracil in its bright (second) electronically excited singlet state. To facilitate a comparison of the calculated RR spectra of uracil, all peak positions, that is, the vibrational frequencies, were calculated with PBE0 at the corresponding optimized ground-state equilibrium structure.

Setting out from the currently accepted, standard active orbital space of 14 electrons in ten orbitals (CAS(14,10)) for uracil, we found that the vertical excitation energy to the bright singlet excited state can be largely improved by augmenting the CAS with Rydberg orbitals (mainly comprised of 3p-type orbitals). Further inclusion of all σ/σ^* skeleton orbitals of the pyrimidine ring led to an unbalanced treatment of nondynamical and dynamical electron correlation contributions, which ultimately resulted in a reversion of the trend with respect to the vertical excitation energies observed for augmentation with Rydberg-type orbitals only.

Based on quantum information measures, we identified a CAS(18,23) orbital space that comprises a set of Rydberg-type orbitals as well as all σ/σ^* skeleton orbitals that are of importance to describe the photophysics of the low-lying electronic singlet excited states of uracil. Consequently, DMRG-SCF calculations with the CAS(18,23) gave not only absolute vertical excitation energies in reasonable agreement with experiment but also yielded an energy gap between the first two excited singlet states that is the closest to its corresponding experimental estimate among all active orbital spaces for DMRG-SCF considered in this work. In view of the above findings and the qualitatively wrong RR spectrum, we consider the accuracy of the CASSCF/CASPT2 vertical excitation energies obtained for the initial CAS(14,10) orbital space to be likely a result of a fortuitous cancellation of errors.

A further comparison of the calculated with the experimental RR spectra allowed us to assess the quality of the DMRG-SCF excited-state gradients obtained for the different choices of the active orbital space. In contrast to the vertical excitation energies, calculations with the full-valence CAS(30,26) gave the best quantitative agreement of the main band intensities in comparison with the experimental RR spectrum. Compared with previous work based on density functional theory calculations, we observed larger deviations from the experimental RR spectrum in particular in the low-frequency part of the RR spectrum. Besides neglecting solvation effects such as hydrogen bonding, the chosen assumptions in our transform theory approach to RR intensities, for example, neither allow for an account of Duschinsky rotations nor of Herzberg–Teller vibronic couplings, where in particular the former could be of significance for a correct intensity distribution of the low-frequency modes (cf. Ref. [10]). Moreover, we further assumed within the IMDHO model that the potential energy surfaces of the ground and excited state are harmonic, which could further contribute to the overestimation of the relative intensities for the low-lying vibrational modes. Although quantitatively less accurate for the prediction of the relative intensities of the main bands in the RR spectrum of uracil compared with the full-valence CAS(30,26), we recommend CAS(18,23) calculations, combined with a subsequent multireference approach to capture dynamical correlation effects, as an appropriate choice while striving for excited-state dynamics of uracil both on short and on long timescales.

Acknowledgments

[1] A. B. Myers, *Chem. Rev.* **1996**, *96*, 911.
[2] K. Kiewisch, J. Neugebauer, M. Reiher, *J. Chem. Phys.* **2008**, *129*, 204103.
[3] C. Herrmann, J. Neugebauer, M. Presselt, U. Uhlemann, M. Schmitt, S. Rau, J. Popp, M. Reiher, *J. Phys. Chem. B* **2007**, *111*, 6078.
[4] J. Guthmuller, B. Champagne, *J. Phys. Chem. A* **2008**, *112*, 3215.
[5] J. Guthmuller, B. Champagne, *J. Chem. Phys.* **2007**, *127*, 164507.
[6] L. Chinsky, A. Laigle, W. L. Peticolas, P.-Y. Turpin, *J. Chem. Phys.* **1982**, *76*, 1.
[7] W. L. Peticolas, T. I. Rush, *J. Comput. Chem.* **1995**, *16*, 1261.
[8] T. I. Rush, W. L. Peticolas, *J. Phys. Chem.* **1995**, *99*, 14647.
[9] L. M. Markham, B. S. Hudson, *J. Phys. Chem.* **1996**, *100*, 2731.
[10] J. Neugebauer, B. A. Hess, *J. Chem. Phys.* **2004**, *120*, 11564.
[11] T. Petrenko, F. Neese, *J. Chem. Phys.* **2012**, *137*, 234107.
[12] S. Luber, J. Neugebauer, M. Reiher, *J. Chem. Phys.* **2010**, *132*, 044113.
[13] J. Guthmuller, B. Champagne, C. Moucheron, A. K. De Mesmaeker, *J. Phys. Chem. B* **2010**, *114*, 511.
[14] F. Santoro, C. Cappelli, V. Barone, *J. Chem. Theory Comput.* **2011**, *7*, 1824.
[15] J. Romanova, V. Liégeois, B. Champagne, *J. Phys. Chem. C* **2014**, *118*, 12469.
[16] J. Romanova, V. Liégeois, B. Champagne, *Phys. Chem. Chem. Phys.* **2014**, *16*, 21721.
[17] S. Sun, A. Brown, *J. Phys. Chem. A* **2014**, *118*, 9228.
[18] A. Baiardi, J. Bloino, V. Barone, *J. Chem. Phys.* **2014**, *141*, 114108.
[19] A. Baiardi, J. Bloino, V. Barone, *J. Chem. Theory Comput.* **2015**, *11*, 3267.
[20] J. Guthmuller, *J. Chem. Phys.* **2016**, *144*, 064106.
[21] K. A. Kramers, W. Heisenberg, *Z. Phys.* **1925**, *31*, 681.
[22] P. A. M. Dirac, *Proc. R. Soc. London Ser. A* **1927**, *114*, 710.
[23] S.-Y. Lee, E. J. Heller, *J. Chem. Phys.* **1979**, *71*, 4777.
[24] E. J. Heller, R. Sundberg, D. Tannor, *J. Phys. Chem.* **1982**, *86*, 1822.
[25] J. Lorentzon, M. P. Fuelscher, B. O. Roos, *J. Am. Chem. Soc.* **1995**, *117*, 9265.
[26] M. Shukla, J. Leszczynski, *J. Comput. Chem.* **2004**, *25*, 768.
[27] T. Pluta, M. Kolaski, M. Medved, S. Budzák, *Chem. Phys. Lett.* **2012**, *546*, 24.
[28] S. Matsika, *J. Phys. Chem. A* **2004**, *108*, 7584.
[29] T. Fleig, S. Knecht, C. Hättig, *J. Phys. Chem. A* **2007**, *111*, 5482.
[30] C. Neiss, P. Saalfrank, M. Parac, S. Grimme, *J. Phys. Chem. A* **2003**, *107*, 140.
[31] B. O. Roos, P. R. Taylor, P. E. Sigbahn, *Chem. Phys.* **1980**, *48*, 157.
[32] P. E. Siegbahn, J. Almlöf, A. Heiberg, B. O. Roos, *J. Chem. Phys.* **1981**, *74*, 2384.
[33] J. Olsen, *Int. J. Quantum Chem.* **2011**, *111*, 3267.
[34] K. Andersson, P.-Å. Malmqvist, B. O. Roos, A. J. Sadlej, K. Wolinski, *J. Phys. Chem.* **1990**, *94*, 5483.
[35] K. Andersson, P.-Å. Malmqvist, B. O. Roos, *J. Chem. Phys.* **1992**, *96*, 1218.

[36] D. Zgid, M. Nooijen, *J. Chem. Phys.* **2008**, *128*, 144116.
[37] D. Ghosh, J. Hachmann, T. Yanai, G. K.-L. Chan, *J. Chem. Phys.* **2008**, *128*, 144117.
[38] F. Aquilante, J. Autschbach, R. K. Carlson, L. F. Chibotaru, M. G. Delcey, L. De Vico, I. F. Galván, N. Ferré, L. M. Frutos, L. Gagliardi, M. Garavelli, A. Giussani, C. E. Hoyer, G. L. Manni, H. Lischka, D. Ma, P. A. Malmqvist, T. Müller, A. Nenov, M. Olivucci, T. B. Pedersen, D. Peng, F. Plasser, B. Pritchard, M. Reiher, I. Rivalta, I. Schapiro, J. Segarra-Martí, M. Stenrup, D. G. Truhlar, L. Ungur, A. Valentini, S. Vancoillie, V. Veryazov, V. P. Vysotskiy, O. Weingart, F. Zapata, R. Lindh, *J. Comput. Chem.* **2016**, *37*, 506.
[39] S. R. White, *Phys. Rev. Lett.* **1992**, *69*, 2863.
[40] S. R. White, *Phys. Rev. B* **1993**, *48*, 10345.
[41] U. Schollwöck, *Rev. Mod. Phys.* **2005**, *77*, 259.
[42] U. Schollwöck, *Ann. Phys.* **2011**, *326*, 96.
[43] Ö. Legeza, R. M. Noack, J. Solyom, L. Tincani in *Computational Many-Particle Physics, Lecture Notes in Physics, Vol. 739* (Eds.: H. Fehske, R. Schneider, A. Weisse), Springer, Heidelberg, **2008**, pp. 653–664.
[44] G. K.-L. Chan, J. J. Dorando, D. Ghosh, J. Hachmann, E. Neuscamman, H. Wang, T. Yanai in *Frontiers in Quantum Systems in Chemistry and Physics, Progress in Theoretical Chemistry and Physics* (Eds.: S. Wilson, P. J. Grout, J. Maruani, G. Delgado-Barrio, P. Piecuch), Springer, Amsterdam, **2008**, pp. 49–65.
[45] G. K.-L. Chan, D. Zgid, *Annu. Rep. Comput. Chem.* **2009**, *5*, 149.
[46] K. H. Marti, M. Reiher, *Z. Phys. Chem.* **2010**, *224*, 583.
[47] K. H. Marti, M. Reiher, *Phys. Chem. Chem. Phys.* **2011**, *13*, 6750.
[48] G. K.-L. Chan, S. Sharma, *Annu. Rev. Phys. Chem.* **2011**, *62*, 465.
[49] S. Wouters, D. van Neck, *Eur. Phys. J. D* **2014**, *68*, 272.
[50] Y. Kurashige, *Mol. Phys.* **2014**, *112*, 1485.
[51] T. Yanai, Y. Kurashige, W. Mizukami, J. Chalupsky, T. N. Lan, M. Saitow, *Int. J. Quantum Chem.* **2015**, *115*, 283.
[52] R. Olivares-Amaya, W. Hu, N. Nakatani, S. Sharma, J. Yang, G. K.-L. Chan, *J. Chem. Phys.* **2015**, *142*, 034102.
[53] S. Szalay, M. Pfeffer, V. Murg, G. Barcza, F. Verstraete, R. Schneider, Ö. Legeza, *Int. J. Quantum Chem.* **2015**, *115*, 1342.
[54] S. Knecht, E. D. Hedegård, S. Keller, A. Kovyrshin, Y. Ma, A. Muolo, C. J. Stein, M. Reiher, *Chimia* **2016**, *70*, 244.
[55] G. K.-L. Chan, A. Keselman, N. Nakatani, Z. Li, S. R. White, *J. Chem. Phys.* **2016**, *145*, 014102.
[56] C. J. Stein, M. Reiher, *J. Chem. Theory Comput.* **2016**, *12*, 1760.
[57] C. J. Stein, V. von Burg, M. Reiher, *J. Chem. Theory Comput.* **2016**, *12*, 3764.
[58] L. B. Clark, G. G. Peschel, I. Tinoco, Jr., *J. Phys. Chem.* **1965**, *69*, 3615.
[59] J. Neugebauer, DNR V1.0—A program for resonance Raman and vibronic structure calculations, ETH Zürich, **2007**.
[60] W. Hu, G. K.-L. Chan, *J. Chem. Theory Comput.* **2015**, *11*, 3000.
[61] T. H. Dunning, Jr., *J. Chem. Phys.* **1989**, *90*, 1007.
[62] R. A. Kendall, T. H. Dunning, Jr., R. J. Harrison, *J. Chem. Phys.* **1992**, *96*, 6796.
[63] J. P. Perdew, M. Ernzerhof, K. Burke, *J. Chem. Phys.* **1996**, *105*, 9982.
[64] J. P. Perdew, K. Burke, M. Ernzerhof, *Phys. Rev. Lett.* **1996**, *77*, 3865.
[65] C. Adamo, V. Barone, *J. Chem. Phys.* **1999**, *110*, 6158.
[66] Gaussian 09 (Revision D.01), M. J. Frisch, G. W. Trucks, H. B. Schlegel, G. E. Scuseria, M. A. Robb, J. R. Cheeseman, G. Scalmani, V. Barone, B. Mennucci, G. A. Petersson, H. Nakatsuji, M. Caricato, X. Li, H. P. Hratchian, A. F. Izmaylov, J. Bloino, G. Zheng, J. L. Sonnenberg, M. Hada, M. Ehara, K. Toyota, R. Fukuda, J. Hasegawa, M. Ishida, T. Nakajima, Y. Honda, O. Kitao, H. Nakai, T. Vreven, J. A. Montgomery, Jr., J. E. Peralta, F. Ogliaro, M. Bearpark, J. J. Heyd, E. Brothers, K. N. Kudin, V. N. Staroverov, R. Kobayashi, J. Normand, K. Raghavachari, A. Rendell, J. C. Burant, S. S. Iyengar, J. Tomasi, M. Cossi, N. Rega, J. M. Millam, M. Klene, J. E. Knox, J. B. Cross, V. Bakken, C. Adamo, J. Jaramillo, R. Gomperts, R. E. Stratmann, O. Yazyev, A. J. Austin, R. Cammi, C. Pomelli, J. W. Ochterski, R. L. Martin, K. Morokuma, V. G. Zakrzewski, G. A. Voth, P. Salvador, J. J. Dannenberg, S. Dapprich, A. D. Daniels, Ö. Farkas, J. B. Foresman, J. V. Ortiz, J. Cioslowski, D. J. Fox, Gaussian Inc., Wallingford, CT, **2009**.
[67] C. Puzzarini, V. Biczysko, V. Barone, *J. Chem. Theory Comput.* **2011**, *7*, 3702.
[68] TURBOMOLE V6.5 2013, a development of University of Karlsruhe and Forschungszentrum Karlsruhe GmbH, **1989**–**2007**, TURBOMOLE GmbH, since **2007**; available from http://www.turbomole.com.
[69] S. Keller, M. Dolfi, M. Troyer, M. Reiher, *J. Chem. Phys.* **2015**, *143*, 244118.
[70] S. Keller, M. Reiher, *J. Chem. Phys.* **2016**, *144*, 134101.
[71] Y. Ma, S. Keller, C. Stein, S. Knecht, R. Lindh, M. Reiher, **2016**, in preparation.
[72] S. Keller, M. Reiher, *Chimia* **2014**, *68*, 200.
[73] G. Barcza, Ö. Legeza, K. H. Marti, M. Reiher, *Phys. Rev. A* **2011**, *83*, 012508.
[74] S. Laimgruber, T. Schmierer, P. Gilch, K. Kiewisch, J. Neugebauer, *Phys. Chem. Chem. Phys.* **2008**, *10*, 3872.
[75] S. Yarasi, S. Ng, G. R. Loppnow, *J. Phys. Chem. B* **2009**, *113*, 14336.
[76] Y. Mercier, F. Santoro, M. Reguero, R. Improta, *J. Phys. Chem. B* **2008**, *112*, 10769.
[77] B. O. Roos, K. Andersson, M. P. Fülscher, *Chem. Phys. Lett.* **1992**, *192*, 5.
[78] L. Serrano-Andrés, B. O. Roos, *J. Am. Chem. Soc.* **1996**, *118*, 185.
[79] R. Improta, V. Barone, *J. Am. Chem. Soc.* **2004**, *126*, 14320.
[80] W. A. Eaton, T. P. Lewis, *J. Chem. Phys.* **1970**, *53*, 2164.
[81] Ö. Legeza, J. Sólyom, *Phys. Rev. B* **2003**, *68*, 195116.
[82] J. Rissler, R. M. Noack, S. R. White, *Chem. Phys.* **2006**, *323*, 519.
[83] Ö. Legeza, J. Sólyom, *Phys. Rev. Lett.* **2006**, *96*, 116401.
[84] K. Boguslawski, P. Tecmer, Ö. Legeza, M. Reiher, *J. Phys. Chem. Lett.* **2012**, *3*, 3129.
[85] B. E. Billinghurst, S. A. Oladepo, G. R. Loppnow in *Radiation Induced Molecular Phenomena in Nucleic Acids* (Eds.: M. K. Shukla, J. Leszczynski), Springer, Amsterdam, **2008**, pp. 237–264.
[86] M.-P. Gaigeot, C. Kadri, M. Ghomi, *J. Mol. Struct.* **2001**, *565*, 469.
[87] M. L. Laury, S. E. Boesch, I. Haken, P. Sinha, R. A. Wheeler, A. K. Wilson, *J. Comput. Chem.* **2011**, *32*, 2339.